Automatic Compensation for Defects of Laser Reflective Patterns in Optics-Based Auto-Focusing Microscopes

Wei-Yen Hsu

***Abstract*—Since the optomechatronic system is characterized by a high energy density and high response speed, system performance can be substantially improved by integrating optical components with electromechanical systems. For micro-processing, conventional machining has been commonly replaced with laser processing. Auto-focusing plays a crucial role in processing, so developing an autofocus (AF) system with high precision and speed is vital. AF modules integrated with the knife edge method typically use a reflective semicircular laser image to calculate the defocus distance for the optical instrument and evaluate the accuracy. On the stage of an optical instrument, a reflective image is typically not a standard semicircular segment because of the different reflection characteristics of objects or the positioning error of the devices. In this study, a novel method is proposed to automatically compensate for these defects and errors. In addition to the compensation part, the improved adaptive anisotropic diffusion filter and wavelet-based edge detection are both proposed for pattern smoothing and enhancement, and pattern edge detection. For reflective patterns obtained using an image sensor in an optics-based AF module, the proposed method, compared with six state-of-the-art approaches in terms of several metrics, such as compensation accuracy, sensitivity, specificity, Dice coefficient, mean absolute distance, Hausdorff distance, and speed / computation time, enables and facilitates accurately reconstructing the complete semicircular segment. Experimental results show that the proposed method yields more satisfactory, stable and accurate results in comparison with six other approaches in performance analysis and statistical evaluation.**

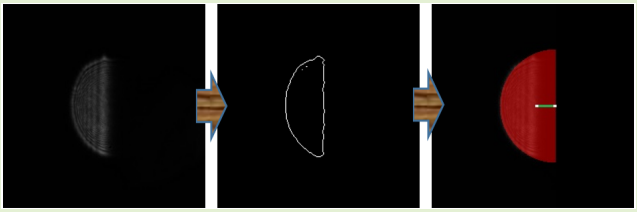

***Index Terms*— Autofocus system, adaptive anisotropic diffusion, compensation, reflective pattern, wavelet.**

I. Introduction

SEMICONDUCTOR microelectronics, micro-electro-mechanics, and laser technology have contributed to the rapid growth of image-display industries. As the production of display panels increases and large-size panels emerge, maintaining and repairing such panels have increased in frequency, in-creasing labor time and material costs. Thus, quality inspection for production lines is imperative. To achieve the purpose of precision machining, autofocus (AF) modules are frequently used to facilitate the machining process [1], [2]. Therefore, an accurate laser AF system is essential for the focusing performance of precision instruments [3], [4].

To achieve a highly efficient process in industrial manufacturing, stringent functional requirements for AF modules are crucial. AF technology and measurement systems are used primarily to calculate the amount of defocus of an object and the relative distance between target objects so that the optical system can move the target object onto the workpiece [5]. In addition, they can be used to adjust the positions of optical lenses to change the distance be-tween the workpiece and lenses, thus enabling the target object to coincide with the work-piece surface [6]. Overall, AF technology has been applied in numerous fields, including laser processing [7], [8], photography, microscopy [9], [10], and light detection devices [11].

Currently, industrial AF modules can be divided into two types. One type is image-based AF methods, which apply image sharpness and image spatial frequency to determine the position of the workpiece before adjusting the relative

Manuscript received June 19, 2019; revised August 28, 2019; accepted October 16, 2019. Date of publication October 23, 2019; date of current version January 24, 2020. This work was supported by the Ministry of Science and Technology, Taiwan, under Grant MOST105-2410-H-194-059-MY3 and Grant MOST108-2410-H-194-088-MY3. The associate editor coordinating the review of this article and approving it for publication was Dr. Francis P. Hindle.

The author is with the Center for Innovative Research on Aging Society, National Chung Cheng University, Chiayi 62102, Taiwan, with the Department of Information Management, National Chung Cheng University, Chiayi 62102, Taiwan, and also with the Advanced Institute of Manufacturing With High-Tech Innovations, National Chung Cheng University, Chiayi 62102, Taiwan (e-mail: shenswy@gmail.com).

Digital Object Identifier 10.1109/JSEN.2019.2949033

positions of a camera and the target object. The capability and speed of image-based auto-focusing depends on the algorithms used [12]. The other type is optics-based AF methods, which determine the defocus distance and direction based on changes in the shape of the laser spot (light energy) detected by an image sensor. The major advantages of optics-based AF methods are high focusing precision and speed [13]. AF systems enhance focusing precision and speed through two approaches: system structure, which involves changing the curvature of the lens surface or relative distance between the lenses to adjust system magnification and improve system performance [14]; and image processing, which involves using algorithms to remove noise and calibrate reflective patterns so that focusing conditions and image clarity can be accurately assessed. Subsequently, signals are sent back to the system to control motor operation, thereby increasing the sensitivity and precision of the AF system [15], [16].

Although the lateral position and size of the reflective pattern provides enough data for the implementation of the auto-focusing, the proposed automatic compensation method can efficiently reduce the number of iterations of auto focusing and simultaneously avoid focus failure and error by improving the reflective patterns in an auto-focusing system. In this study, a novel method is proposed to automatically compensate for the aforementioned defects and errors. Laser images subjecting to various influences were processed using the proposed method. Subsequently, a complete semicircular segment was constructed to accurately calculate the distance between the centroid and center point (i.e., center-to-centroid distance), thereby facilitating a rapid automatic calibration of the AF module.

The remainder of this study is organized as follows: we review related work in Section 2. In Section 3, we describe our proposed system for automatic defect compensation in laser reflective patterns, and in Section 4, we detail our experimental evaluation. Lastly, in Section 5, we offer our conclusions for future research.

II. Related Work

Variations in laser images influence the performance assessment of optics-based AF methods. Therefore, in analyzing such variations, some studies have employed quadrant photodiode in an AF module to detect changes in the shape of the astigmatism spot and to establish a focus-error function for calculating the defocus distance of the target object [17]. Moreover, image fusion technology was employed to produce a high-resolution image from an image sequence. Subsequently, subpixel edge detection was conducted to identify ellipse features from the high-resolution image. These ellipse features were then projected into a three-dimensional space to obtain appropriate circular features, thus enhancing the focus of the test system [18]. In addition, the pixel-difference method and band-pass-energy method were proposed for inspecting image clarity. The methods integrate frequency-domain filtering with pixel difference to increase image clarity and determine the optimal focusing position [19].

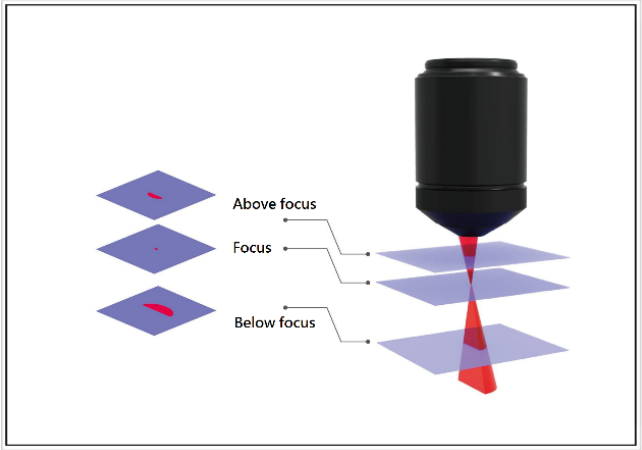

Fig. 1. Focusing condition is influenced by the position of workpiece.

(a) (b)

Fig. 2. Reflective patterns. (a) When the workpiece is located between the lens and focal point, (b) when the workpiece is placed far from the focal point.

The optics-based auto-focusing microscope that applies the knife edge method was adopted in this study. During the focusing process, the reflected light was cut off by the knife, resulting in variations in the emitted light, the pattern of which then changed on the detection surface of a charge-coupled device sensor. Subsequently, the detected light intensity was used to calculate focus error, which served as the basis for focusing. In particular, the position of the workpiece significantly influences the focusing condition, as shown in Fig. 1. When the workpiece is not aligned with the focal point, the reflective image will be defocused or the reflection area will be enlarged, generating blurred images [20], [21]. When the workpiece is located between the lens and focal point, a semicircular reflective pattern is projected on the left, as shown in Fig. 2(a). When the work piece surface is placed far from the focal point, a corresponding pattern is projected on the right, as shown in Fig. 2(b). According to the theory of triangulation [22], the radius and area of the semicircular reflective pattern increase as the distance between the workpiece and focal point increases.

According to Lasinski [23], when the imaging capability of an AF module is within a linear range, the centroid coordinates of an image can be used to measure the defocus distance and direction of the optical patterns. Wang et al. adopted the centroid coordinates of an image to adjust the position of lenses in AF modules [24]. The conventional centroid

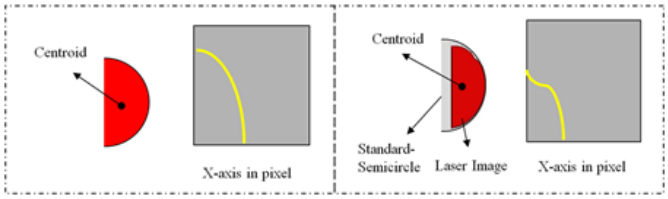

Fig. 3. Position of gravity center of reflective pattern. (a) Complete semicircle (ideal condition), (b) non-complete semicircle (under inference).

algorithm [25] involves estimating the centroid position of an image by using the coordinates and intensity values of all the pixels of the image.

$$X_{centroid} = \frac{\sum\sum (x - x_c)\, P_{ij}}{\sum\sum P_{ij}} \tag{1}$$

$$Y_{cenroitd} = \frac{\sum\sum (y - y_c)\, P_{ij}}{\sum\sum P_{ij}} \tag{2}$$

where x and x_c represent x-coordinate of each pixel and the centroid, whereas y and y_c stand for y-coordinate of each pixel and the centroid; P_{ij} represents the intensity of each pixel in the semicircular segment. During the operation process, the optics-based AF module is easily influenced by light interference, object reflection, energy loss, and errors in device positioning. Any of these factors can cause the obtained image to demonstrate uneven brightness, excess noise, and fragmented patterns, significantly influencing the projection result produced by an optical instrument. Therefore, when a laser beam passes through the focusing camera and focuses on a workpiece, the reflective pattern is not a semicircular segment because of the aforementioned factors, as shown in Fig. 3. When the pixels of the semicircular segment (P_{ij}) are evenly distributed, the positions of the semicircle centroid and center point (i.e., displacement and defocus distance) show a linear change. However, when a laser image is influenced by pattern shift, small deformation, and interference, using Eq. (1) and (2) to estimate the centroid position is likely to produce an incorrect result, hindering defocus distance calculations. To overcome the above-described defects in laser reflective patterns, several compensation approaches have been published [25]–[29]. An improved algorithm [26] is based on an immersion process analogy, in which the flooding of the water in the pattern is efficiently simulated using of queue of pixel. A region growing algorithm [29] is proposed to use the pixel centers as seeds that fill the holes where no data was observed to recover a defect representation. An image segmentation algorithm using local binary fitting (LBF) active contour model [28] is employed to process the laser range image to characterize anomalies in the pipe profile to extract geometric information from the pre-processed laser profile. A least squares fitting algorithm [27] is used to compute the circle/ellipse for which the sum of the squares of the distances to the given points is minimal. The comparisons among the above-mentioned related work and their various influence are listed in Table I. However, these approaches still produce imperfect results in defect compensation. Therefore, a novel method, which can process various influence, is proposed to automatically compensate for the aforementioned defects in this study.

TABLE I
COMPARISONS AMONG RELATED WORK AND THEIR VARIOUS INFLUENCE

Related Work	Various Influence
Reed & Hutchinson [18]	● Image fusion technology is employed to produce a high-resolution image from an image sequence. ● Subpixel edge detection is then conducted to identify ellipse features from the high-resolution image. ● These ellipse features are projected into a three-dimensional space to obtain appropriate circular features, thus enhancing the focus of the test system
Kesseler & Fischer [19]	● The pixel-difference method and band-pass-energy method are proposed for inspecting image clarity. ● The methods integrate frequency-domain filtering with pixel difference to increase image clarity and determine the optimal focusing position.
Birch et al. [26]	● An improved algorithm is based on an immersion process analogy, in which the flooding of the water in the pattern is efficiently simulated using of queue of pixel.
Chernov & Lesort [27]	● A least squares fitting algorithm is used to compute the circle/ellipse for which the sum of the squares of the distances to the given points is minimal.
Liu & Krys [28]	● An image segmentation algorithm using local binary fitting (LBF) active contour model is employed to process the laser range image to characterize anomalies in the pipe profile to extract geometric information from the pre-processed laser profile.
Xiong et al. [29]	● A region growing algorithm is proposed to use the pixel centers as seeds that fill the holes where no data was observed to recover a defect representation.

III. MATERIALS AND METHODS

The research flow adopted in this study is shown in Fig. 4. For a laser image containing defects, the improved adaptive anisotropic diffusion filter is proposed for pattern smoothing and enhancement. The threshold discrimination method and morphology closing are then used to binarize pattern and remove holes to provide connectivity between components. Next, wavelet-based edge detection is proposed for pattern edge detection. Finally, we applied the proposed compensation method for pattern defects to automatically compensate for the laser reflective pattern to generate a complete semicircular segment, which was then employed to calculate the correct centroid position and thereby obtain the center-to-centroid distance.

A. Materials

The optical module of single-layer laser AF system was used to obtain the laser reflective pattern, the size of which is 256 × 256 pixels. The pattern was the area projected on the sensor by light and can be classified into images of inner focus and outer focus with a focal length range between −300 and 300 μm at an interval of 10 μm. In the study, twenty pattern/image sequences were used, wherein ten image sequences were obtained from optical path I, while another ten image sequences were obtained from optical path II. Each pattern/image sequence consisted of 61 patterns, including

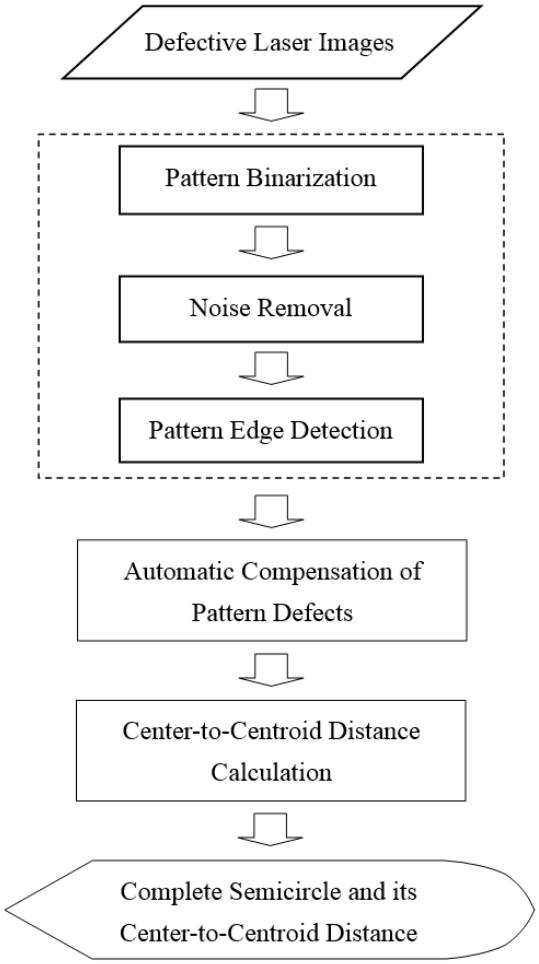

Fig. 4. Flowchart of the proposed system.

both the inner-focus and outer-focus images. The patterns with defects were employed for compensation and then evaluation during the experiments.

B. Pattern Smoothing and Enhancement

There exist a lot of defects, noise and artifacts in the laser reflective patterns, as shown in Fig. 2, so the traditional smoothing approaches, such as Gaussian filtering and mean filtering, can't work well on smoothness. In addition, these filters don't also reserve and even enhance the edges while performing the image blurring and smoothing. The anisotropic diffusion filter is a kind of non-linear filter that calculates the pixel value by considering the non-linear relationship between the target and adjacent pixels. More specifically, the pixel value is evaluated by means of a monotonic descent function, which calculates the proportion of gradients between the center target pixel and the adjacent pixel with a non-linear function, and they are combined into a new pixel value. Although the traditional smoothing approaches use the weighted mask to smooth the image, which are similar to the concept of nonlinear diffusion, the ability of edge preserving of nonlinear diffusion is strongly better. Since different gradients are taken into account for the nonlinear function when it calculates the new pixel value, it can achieve the purpose of removing the noise and preserving the detailed information of edges.

Anisotropic diffusion was firstly proposed by Perona and Malik [30], and then enhanced by Chao and Tsai [31]. In this study, we propose an improved anisotropic diffusion to further make it adaptive by adding three novel ideas. Firstly, the neighborhoods are extended from four directions to eight directions. Next, the weights of neighborhoods are considered and added to distinguish between the boundary and background. Finally, the judgment smoothing or sharpening mechanism is added after the novel diffusion model is performed. The anisotropic diffusion equation is defined as follows,

$$\frac{\partial I}{\partial t} = div\left(c(|\nabla I|)\nabla I\right) \tag{3}$$

where I represents the original color image, ∇ is the gradient operator, div means the divergence, and $c(|\nabla I|)$ stands for the diffusion function, in which the diffusion rate is adjusted. That is, the gradient function of image is carefully selected, so that the edge of images can be preserved under diffusion. The steps are described in detail as follows:

Firstly, the gradients in eight directions are calculated. More specifically, the information of image gradients is considered and expanded from the traditional four directions to eight neighborhoods, making the image be capability of better edge preserving and noise suppression.

Next, the diffusion functions of smoothing and sharpening are calculated. Inspired from the concept of edge probability density function, the smooth diffusion function is proposed and defined as,

$$c(|\nabla I|) = \alpha \sin^2\left(\frac{\pi}{2}e^{-(|\nabla I|/k)^2}\right) \tag{4}$$

where k is used to adjust the gradient function $|\nabla I|$, and the weighted parameter α is defined for the eight directions, whose values are varies inversely to the oblique direction. In addition, a novel sharpening diffusion function is also proposed to sharpen larger gradient areas while smoothing. which is defined as,

$$c(|\nabla I|) = \beta \cos^2\left(\frac{\pi}{2}e^{-(|\nabla I|/k)^2}\right) \tag{5}$$

where the weighted parameter β is defined for the eight directions, whose values are inverse to the reciprocal of distances between the four neighborhoods and the oblique direction. Moreover, the average of gradient variety of eight directions is used to determine the regions, which is suitable to be smoothed or sharpened under diffusion, as described in the following,

$$\begin{aligned} &if(\nabla I \le (\textstyle\sum_{i=1}^{8} \nabla I_i)/8) \\ &c(|\nabla I|) = \alpha \sin^2\left(\frac{\pi}{2}e^{-(|\nabla I|/k)^2}\right) \\ &else \\ &c(|\nabla I|) = \beta \cos^2\left(\frac{\pi}{2}e^{-(|\nabla I|/k)^2}\right) \end{aligned} \tag{6}$$

Finally, the first and second steps are performed iteratively,

$$I = I_0 + \lambda \sum_{i=1}^{8} \left(c(|\nabla I_i|)\nabla I_i\right) \tag{7}$$

where λ is used to adjust the diffusion rate. Fig. 5(a) shows an initial laser image (200 μm) that contains defects,

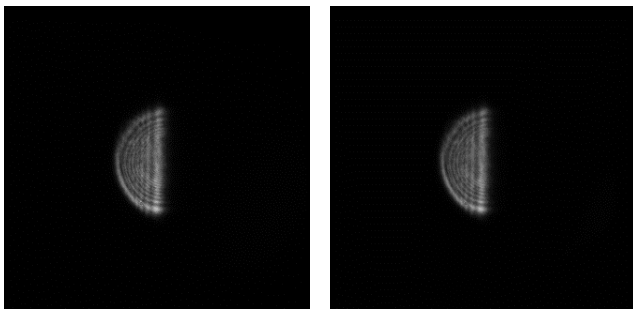

(a) (b)

Fig. 5. Result of pattern smoothing and enhancement. (a) Initial laser image (200 μm), (b) pattern smoothing and enhancement.

(a) (b)

Fig. 6. Results of pattern binarization and morphology closing. (a) Pattern binarization, (b) binary image morphology closing.

and Fig. 5(b) demonstrates the result of image smoothing and enhancement. The proposed improved adaptive anisotropic diffusion filter is employed because it is capable of eliminating the outlier pixels on the edge of the semicircular reflective pattern while maintaining the sharpness of the edge.

C. Pattern Binarization and Morphology Closing

The objective of binarization was to place all the pixels of an image onto the grey-level histogram, segmenting the image into the area of interest and background [32]. A laser image consists of areas in which light reflection and no reflection are presented; however, it typically features uneven brightness. Optical microscope settings may influence the resulting images. Specifically, when the focal length of a lens is short, a bright image with compact structures is generated. By contrast, a long focal length yields dim images with loose structure and blurred edge. To achieve satisfactory segmentation, the threshold discrimination method [33] is adopted for pattern binarization in this study. Fig. 6(a) shows the result of pattern binarization by the threshold discrimination method, and Fig. 6(b) demonstrates the result of morphology closing. The threshold discrimination method can resolve the problems of few color variations and image blocks in laser images as well as perform favorably in terms of time complexity, whereas morphology closing can remove gaps and holes and provide connectivity between components.

D. Pattern Edge Detection

The use of edge detection is aimed at locating the boundary pixels, the grey level of which changed considerably, to eliminate irrelevant data and retain the pattern edge. Edge is considered a crucial factor for the proposed automatic compensation of pattern defects. Edge detection means extracting important boundary information from the images. Multiresolution image decomposition is an effective approach in analyzing image properties. In this study, wavelet-based edge detection is proposed to detect edge points with strong and consistent responses to capture the edge of the semicircular reflective pattern on the laser image.

A 2D wavelet transform [34] in each level is expressed as the tensor product of two 1D wavelet transforms that are orthogonal to each other due to its separable characteristic. Let $\phi^H(x,y) = \frac{\partial S(x,y)}{\partial x}$ and $\phi^V(x,y) = \frac{\partial S(x,y)}{\partial y}$, where $S(x,y)$ is a 2D smoothing function, stand for two 1D wavelet functions in the x and y directions, respectively. We denote $\xi_j(x,y) = \frac{1}{2^{2j}}\xi(\frac{x}{2^j}, \frac{y}{2^j})$, which is the dilation by a scaling factor j of any 2D $\xi(x,y)$ function. The mathematical equations for 2D wavelet transform of an image $f(x,y)$ are described in detail as follows,

$$W_j^H f(x,y) = f * \phi_j^H(x,y) = f * (2^j \cdot \frac{\partial S_j}{\partial x})(x,y) = 2^j \cdot \frac{\partial}{\partial x}(f * S_j)(x,y),$$

and

$$W_j^V f(x,y) = f * \phi_j^V(x,y) = f * (2^j \cdot \frac{\partial S_j}{\partial y})(x,y) = 2^j \cdot \frac{\partial}{\partial y}(f * S_j)(x,y), \quad (8)$$

where $W_j^H f(x,y)$ and $W_j^V f(x,y)$ represent the gradient of image $f(x,y)$ in the x and y directions at level j, respectively. Next, the gradient modulus is derived as

$$M_j f(x,y) = \sqrt{\left| W_j^H f(x,y) \right|^2 + \left| W_j^V f(x,y) \right|^2} \quad (9)$$

All the edge points in image $f(x,y)$ at level j can be detected after a predefined threshold is used. In addition, noise is an important factor that leads to false detection of edge points and can be easily filtered out by a process of multiscale edge confirmation. Accordingly, a wavelet-based edge detection is proposed to make the edge detection more reliable by suppressing the influence of noise.

$$R_n(j,x,y) = \prod_{i=0}^{n-1} M_{j+i} f(x,y) \quad (10)$$

where n is the number of multiplication scale and j is the initial level. By means of proposed wavelet-based edge detection, edge points can be distinguished from the noise. That is, edge points can usually exist in multi-scale domain, whereas noise cannot. In this study, this property is applied to detect edge points. The product of the gradient moduli in multiscales is used to determine the edge points from the laser images. The result of edge point detection is shown in Fig. 7.

E. Automatic Compensation of Pattern Defects

After the edge of the reflective pattern was obtained, the proposed automatic compensation method for pattern defects was

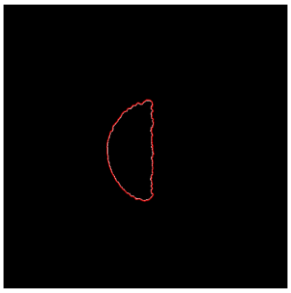

Fig. 7. Result of pattern edge detection.

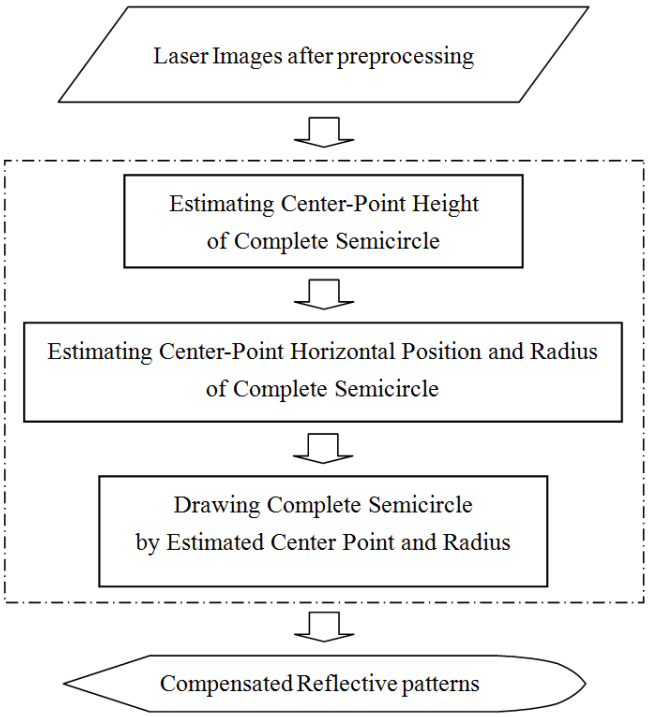

Fig. 8. Flowchart of automatic compensation method for pattern defects.

used to automatically compensate for the reflective pattern and subsequently obtain a complete semicircular segment. The procedure is illustrated in Fig. 8. Specifically, the height of the center point of the complete semicircular segment, its horizontal position, and the radius of the semicircular segment were sequentially estimated. The estimated center point and radius were then used to draw the complete semicircle to generate a compensated reflective pattern.

The procedure of the proposed method is explained in detail as follows: The center point position of the complete semicircle and its radius were calculated using the points on the circumference as well as those on the edge of the reflective pattern. As shown in Fig. 9, the edge of the yellow area consists of the edge points of the reflective pattern. The semicircular segment comprising blue and yellow areas is the complete semicircle produced using the pro-posed method. The steps for the estimation are detailed in the following subsections.

1) Estimating the Center-Point Height of the Complete Semicircular Segment (y-Coordinate): The x-axis and y-axis denote the horizontal and vertical directions, respectively. The yellow

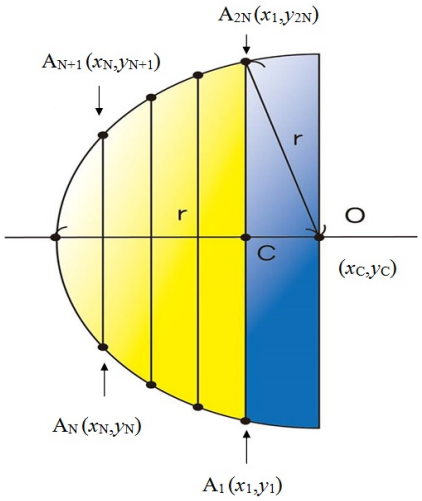

Fig. 9. Diagram of estimation of complete semicircular segment.

semicircle was divided into N blocks by using N-1 vertical cutting lines ($N \geq 2$). The horizontal distance between each block was identical. Subsequently, the upper and lower ends of the lines were identified on the edge of the yellow semicircle; for example, $A_1 = (x_1, y_1)$, and $A_{2N} = (x_1, y_{2N})$. Therefore, the midpoints of the lines were identified, which were then averaged to obtain the y-coordinate for the center point of the complete semicircular segment, as ex-pressed in Eq. (11).

$$y_c = \frac{\sum_{i=1}^{N} \frac{y_i + y_{2N-i+1}}{2}}{N} = \sum_{i=1}^{N} \frac{y_i + y_{2N-i+1}}{2N} \tag{11}$$

If the number of vertical cutting lines increases (i.e., the value of N increases), the accuracy of the estimated y_c increases. In other words, when more edge points were considered, the height of the center point (and thus the correct position of the center point) was prone to in-fluences from outliers.

2) Estimating the Center-Point Horizontal Position (x-Coordinate) and Radius of the Complete Semicircular Segment: After the y-coordinate (y_c) was obtained, the x-coordinate (x_c) of the center point as well as the radius of the semicircular segment were estimated. The y-coordinate of Point C was used as the reference point for equiangular division. Specifically, the angle of a semicircle is 180°, which was divided equiangularly by a unit of z°. Therefore, a total of $(\frac{180}{z} + 1)$ points were labeled on the yellow semicircle (i.e., the incomplete semicircle). For example, if 10° was used as the unit for equiangular division, a total of 19 points would be labeled on the semicircular segment, as shown in Fig. 10. These points (Di) were located on the edge of the yellow semicircle, where $i = 1, 2, \ldots, 19$, and $x_{D_i} = x_{D20-i}$. The height of D_{10} (i.e., the value of the y-coordinate) was identical to that of the center point (O) and point C.

Because D_{10} was at the same height as O, the length of the horizontal radius could be estimated. According to the Pythagorean theorem, each Di ($i = 1 \sim 19$, $i \neq 10$) and D_{10} can be used to separately calculate the x-coordinate (xi) for the center point of a complete semicircular segment.

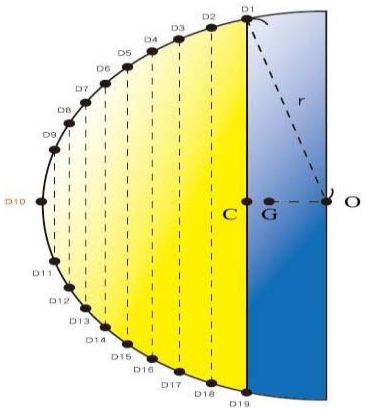

Fig. 10. Diagram of estimation approach.

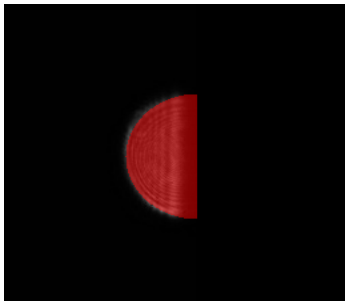

Fig. 11. Result after compensation (red area).

In addition, the outliers can be removed to ensure satisfactory results of xi. However, if removing outliers is not considered, the x-coordinate for the center point of the complete semicircular segment is calculated using Eq. (12).

$$x_c = \frac{1}{18} \sum_{i=1, i\neq 10}^{19} x_i \tag{12}$$

The value x_c (outliers excluded) becomes more accurate as the number of points $(\frac{180}{z} + 1)$ on the yellow semicircle increases. Subsequently, the distance (R_i) between every D_i $(i = 1, 2, \ldots, 19)$ and O can be calculated using the Euclidean distance formula. The radius of the complete semicircular segment was calculated using Eq. (13).

$$r = \frac{1}{19} \sum_{i=1}^{19} R_i = \frac{1}{19} \sum_{i=1}^{19} \|D_i - O\| \tag{13}$$

3) Drawing the Complete Semicircular Segment by Using the Estimated Center Point and Radius: The complete semicircular segment can be produced using the estimated center point O (x_c, y_c) and radius r. In Fig. 11, the red area shows the resulting image after compensating the initial image shown in Fig. 5(a).

F. Center-to-Centroid Distance Calculation

In the complete semicircular segment, G denotes the position of the centroid. Therefore, the center-to-centroid distance $(\overline{OG})$ was calculated using Eq. (14), and O and G were labeled on the semicircular segment.

$$\overline{OG} = \frac{2}{3} + \frac{r \sin\frac{1}{2\pi}}{\frac{1}{2}\pi} = \frac{4r}{3\pi} \tag{14}$$

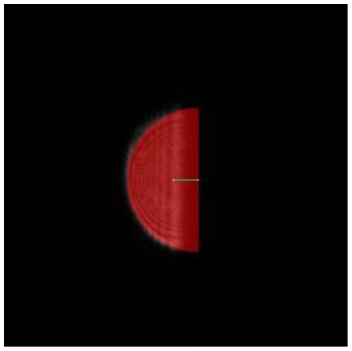

Fig. 12. Calculation of the center-to-centroid distance.

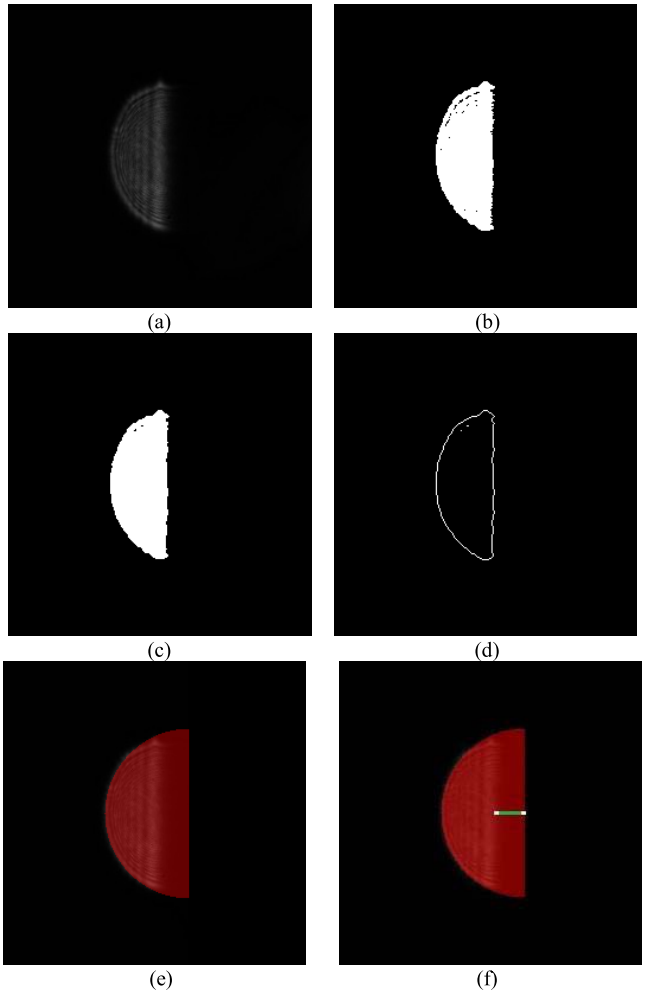

Fig. 13. Intermediate results of the proposed method. (a) Initial laser image (300 μm), (b) pattern binarization, (c) noise removal, (d) pattern edge detection, (e) pattern compensation (red area), (f) calculation of the center-to-centroid distance.

Fig. 12 shows the calculation result of the center-to-centroid distance based on Fig. 11.

IV. Results and Discussion

A. A Case of Compensation

To show the performance of the proposed method, this section delineates the process of the compensation for the initial laser image (300 μm), as shown in Fig. 13. The initial

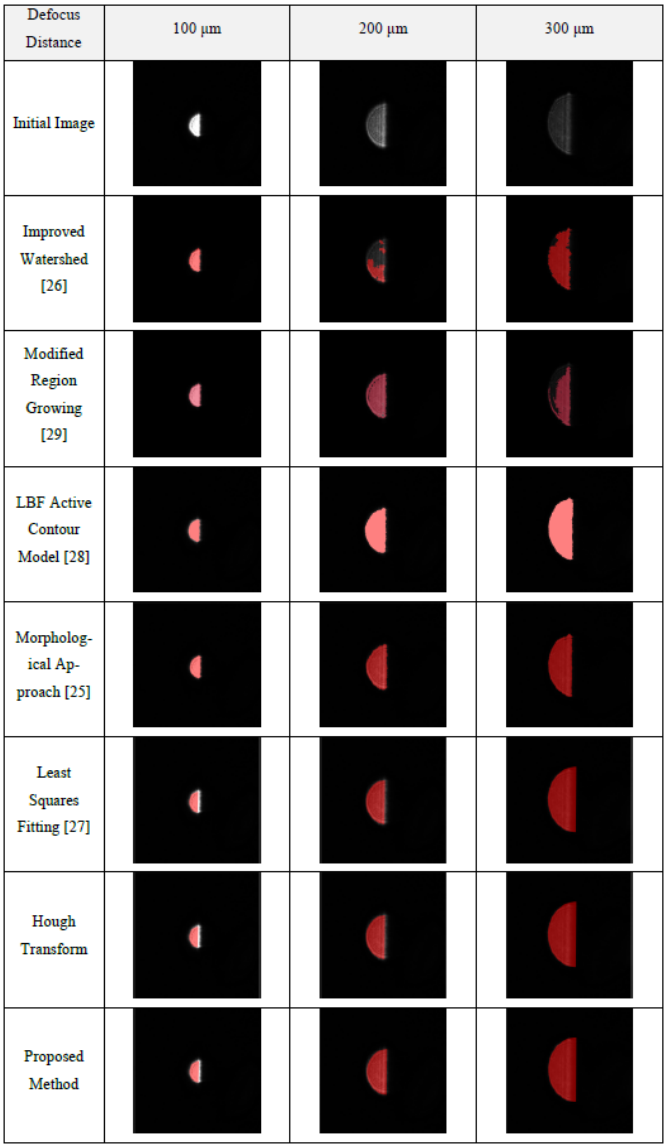

Fig. 14. Pattern compensation results of inner-focus images in optical path I using the proposed method and six other approaches.

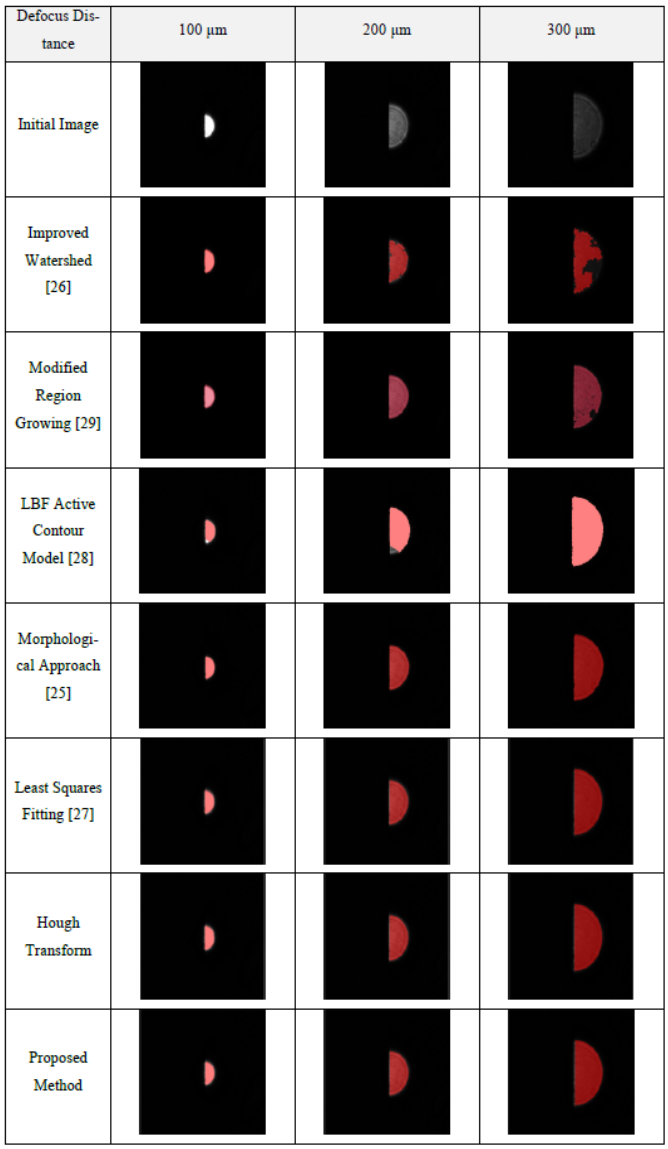

Fig. 15. Pattern compensation results of outer-focus images in optical path I using the proposed method and six other approaches.

laser image is first smoothed and enhanced by the proposed improved adaptive anisotropic diffusion filter, which can simultaneously remove the noise and preserve the edges. Pattern binarization and morphology closing are then performed to remove the holes to separate the pattern and background and retain the pattern structure. Next, wavelet-based edge detection is proposed to obtain data of the pattern edge. Finally, the proposed method, that is, the automatic compensation of pattern defects, is performed to automatically reconstruct a complete semicircular segment (indicated by the red area). This semicircular segment is overlapped on the initial image to examine the degree of coincidence and calculate the center-to-centroid distance.

B. Comparisons With Six State-of-the-Art Approaches

To evaluate the quality and accuracy of the compensation, the proposed method is com-pared with six state-of-the-art approaches [25]–[29]. The experiments are conducted involving various defocus distances to compare the accuracy of the semicircular segments that are compensated using these six methods for visual presentation. The experiment images are laser images of inner and outer focus with a focal length range between -300 and 300 μm. Figures 14 and 15 illustrate the compensation results of inner-focus and outer-focus images for optical path I image sequence using the proposed method and six state-of-the-art approaches, respectively. The compensation results of inner-focus and outer-focus images in optical path II are compared using the proposed method and six other approaches, as shown in Figures 16 and 17, respectively. The results indicate that the compensation efficacy of the proposed method is superior to that of other approaches in both of the optical path I and II.

C. Performance Analysis

Several metrics, including compensation accuracy, sensitivity, specificity, Dice coefficient [35], mean absolute

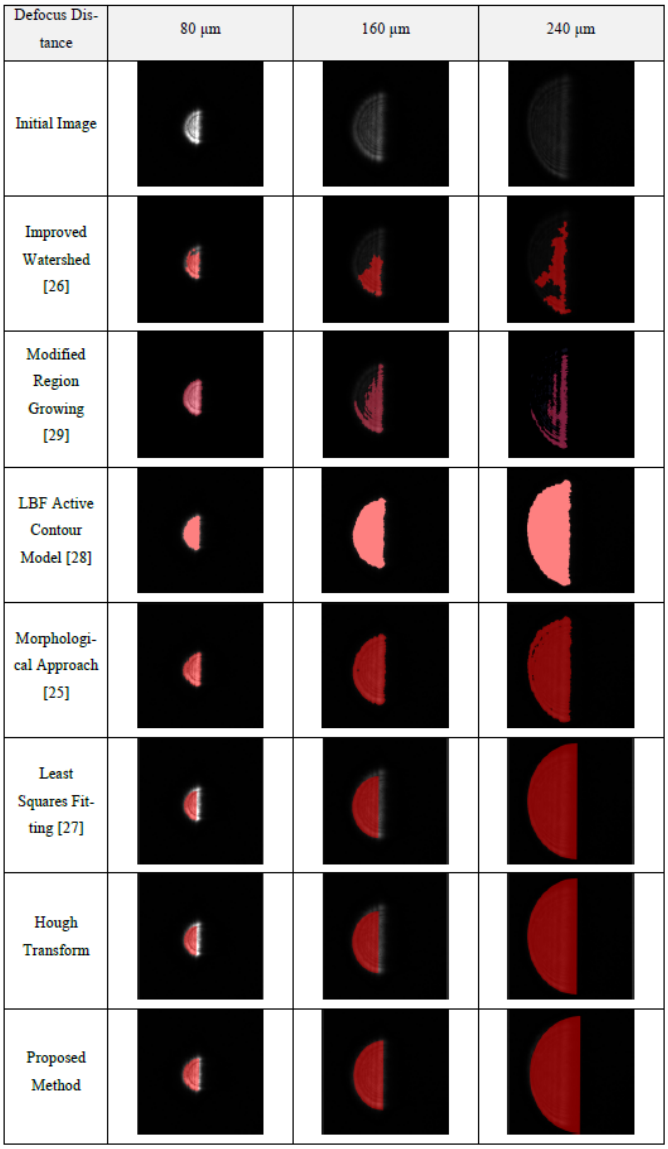

Fig. 16. Pattern compensation results of inner-focus images in optical path II using the proposed method and six other approaches.

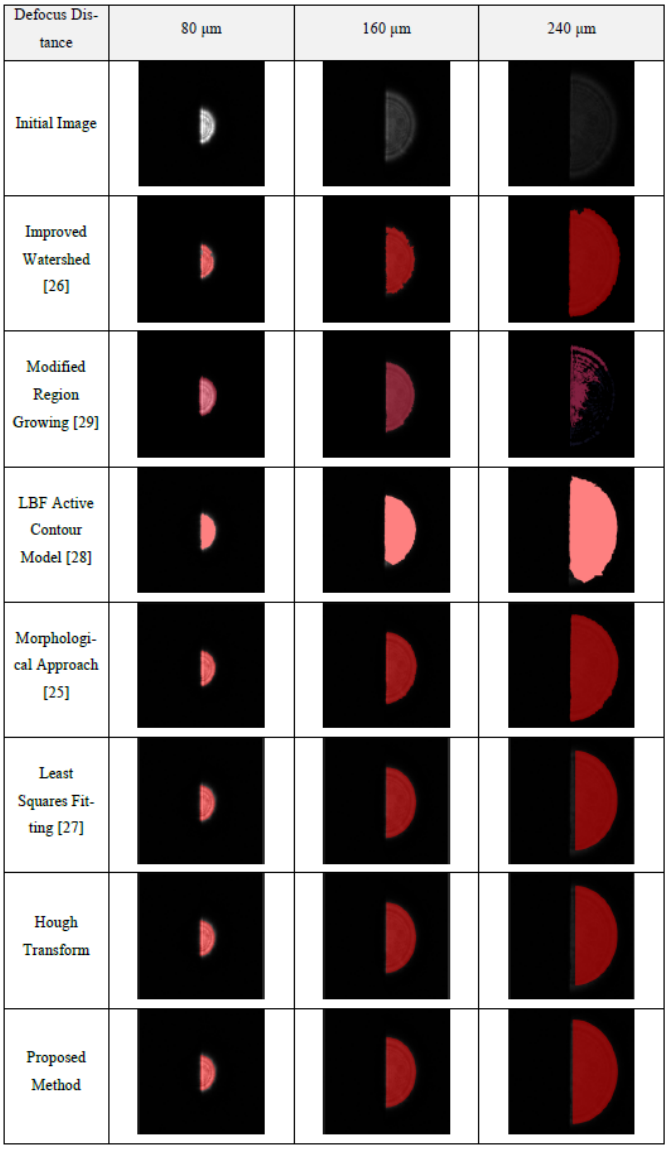

Fig. 17. Pattern compensation results of outer-focus images in optical path II using the proposed method and six other approaches.

distance (MAD) [36], Hausdorff distance [37], and speed / computation time are used to evaluate the performance of these six compensation algorithms. The average compensation accuracy, sensitivity, specificity, Dice coefficient, MAD, Hausdorff distance, and speed / computation time of these six compensation algorithms for both the optical path I and II image sequences, including the images of inner focus and outer focus, are listed in Table II. The results indicate that the proposed meth-od is better than the six state-of-the-art approaches.

D. Statistical Evaluation

To validate whether these six algorithms are significantly different or not, two-way ANOVA and multiple comparison tests are performed for the analysis of all the estimated metrics on the compensation area of both the optical path I and II image sequences, including images of inner focus and outer focus. The statistical analyses with two-way ANOVA are used to evaluate if the differences are significant for the factors' "metrics" and "approaches".

We obtain p-value less than 0.01 for optical path I patterns and less than 0.05 for optical path II patterns on the compensation area. The results of the test indicate that these six algorithms are significantly different. More detailed comparisons of p-values among them are then performed. The results indicate that there are significant differences in the estimation of optical path I patterns between "improved watershed and the proposed method (p-value < 0.01)", "modified region growing and the proposed method (p-value < 0.01)", "LBF active contour model and the proposed method (p-value < 0.05)", and "morphological approach and the proposed method (p-value < 0.05)". In addition, the results also denote that the estimation of optical path II patterns between "improved watershed and the proposed method (p-value < 0.01)", "modified region growing and the proposed method (p-value < 0.01)", "LBF active contour model and the proposed method (p-value < 0.01)", "morphological approach

TABLE II
COMPARISON OF AVERAGE COMPENSATION ACCURACY, SENSITIVITY, SPECIFICITY, DICE COEFFICIENT, MAD, HAUSDORFF DISTANCE AND SPEED/COMPUTATION TIME FROM BOTH OF THE OPTICAL PATH I AND II (INCLUDING INNER-FOCUS AND OUTER-FOCUS) IMAGE SEQUENCES FOR THESE SIX COMPENSATION ALGORITHMS

		Improved Watershed [26]	Modified Region Growing [29]	LBF Active Contour Model [28]	Morphological Approach [25]	Least Squares Fitting [27]	Hough Transform	Proposed Method
Optical Path I Image Sequences	Accuracy	81.01%	85.34%	86.42%	86.89%	96.91%	91.34%	99.40%
	Sensitivity	75.47%	82.46%	87.40%	85.13%	97.13%	89.93%	99.27%
	Specificity	93.14%	95.64%	82.17%	89.40%	96.50%	90.78%	99.54%
	Dice Coefficient	76.95	88.42	91.83	89.20	94.17	92.42	98.81
	MAD	48.15	49.70	49.13	79.19	41.42	46.79	35.47
	Hausdorff Distance	287.87	287.84	283.14	288.42	276.12	279.92	265.87
	Speed / Computation Time	6.63s	4.44s	2.13s	2.76s	0.57s	0.37s	0.04s
Optical Path II Image Sequences	Accuracy	76.63%	78.62%	82.07%	82.66%	92.46%	87.66%	99.07%
	Sensitivity	68.22%	72.82%	83.80%	79.64%	91.04%	86.14%	98.76%
	Specificity	95.67%	94.07%	78.82%	87.81%	95.73%	92.23%	99.30%
	Dice Coefficient	74.48	83.65	92.47	89.66	92.88	91.83	97.88
	MAD	42.98	49.46	35.12	55.23	34.56	35.42	29.35
	Hausdorff Distance	268.52	272.37	243.58	254.59	240.26	244.62	234.28
	Speed / Computation Time	11.83s	7.79s	2.89s	4.21s	0.73s	0.44s	0.05s

and the proposed method (p-value < 0.01)", and "least squares fitting and the proposed method (p-value < 0.05)" are all significantly different. However, the differences of optical path I pat-terns (p-value > 0.05) and optical path II patterns between the LBF active contour model and morphological approach are both not significant. Accordingly, the proposed method obtains the promising performance in the evaluation of six metrics for the defect compensation of laser reflective patterns in optics-based auto-focusing microscopes.

V. CONCLUSION

This study proposes a novel method of automatic compensation for pattern defects, integrating it with images captured using the optics-based AF module to develop a practical precision system that can facilitate determining focusing performance by using data of reflective semicircular segments (e.g., radius and centroid). In this study, we estimated the center-to-centroid distance and examined the linear relationship between the defocus and center-to-centroid distances to accurately and rapidly determine the movement direction of the AF system. Therefore, researchers can use the optical instrument for rapid focusing, detection, and analysis to obtain relevant data for decision making. The experiment result and curvilinear relationship between the center-to-centroid distance and defocus distance revealed that the proposed method can more accurately and effectively compensate the defects in laser images, compared with six state-of-the-art approaches in terms of several metrics, such as compensation accuracy, sensitivity, specificity, Dice coefficient, mean absolute distance, Hausdorff distance, and speed / computation time.

Optical inspections are a highly complex process that must be performed with precision and require expensive materials and processing equipment. Therefore, using low-precision instruments might result in major financial losses. In this study, we processed laser images using the proposed method and then applied them to an AF system, which generated accurate results rapidly. Thus, the proposed method can contribute to the optical inspection industry.

REFERENCES

[1] A. Pentland, T. Darrell, M. Turk, and W. Huang, "A simple, real-time range camera," in *Proc. IEEE Comput. Soc. Conf. Comput. Vis. Pattern Recognit.*, Jun. 1989, pp. 256–261.

[2] T. Starner *et al.*, "Wearable computing and augmented reality," MIT Media Lab Vis. Model. Group, Media Lab., Massachusetts Inst. Technol., Cambridge, MA, USA, Tech. Rep. 355, Nov. 1995.

[3] K.-H. Liu, A. Wiesel, and D. C. Munson, "Synthetic aperture radar autofocus based on a bilinear model," *IEEE Trans. Image Process.*, vol. 21, no. 5, pp. 2735–2746, May 2012.

[4] M. Hamada, A. Kinba, H. Ootsuka, K. Sugitani, and H. Ueda, "Auto focus detecting device comprising both phase-difference detecting and contrast detecting methods," U.S. Patent 5 597 999, Jan. 28, 1997.

[5] K. Campbell, Y. Fainman, and A. Groisman, "Pneumatically actuated adaptive lenses with millisecond response time," *Appl. Phys. Lett.*, vol. 91, Oct. 2007, Art. no. 171111.

[6] Y. Ren *et al.*, "Adaptive-optics-based simultaneous pre-and post-turbulence compensation of multiple orbital-angular-momentum beams in a bidirectional free-space optical link," *Optica*, vol. 1, no. 6, pp. 376–382, 2014.

[7] T.-K. Liu, D. H. Al-Janan, H.-S. Shen, and P.-W. Hsueh, "Optimizing adjustable parameters of servo controller by using unineuro-HUDGA for laser-auto-focus-based tracking system," *IEEE Access*, vol. 5, pp. 823–832, 2017.

[8] W.-Y. Hsu, "Automatic atrium contour tracking in ultrasound imaging," *Integr. Comput.-Aided Eng.*, vol. 23, no. 4, pp. 401–411, 2016.

[9] C.-H. Huang, S. Sankaran, D. Racoceanu, S. Hariharan, and S. Ahmed, "Online 3-D tracking of suspension living cells imaged with phase-contrast microscopy," *IEEE Trans. Biomed. Eng.*, vol. 59, no. 7, pp. 1924–1933, Jul. 2012.

[10] W.-Y. Hsu, "A hybrid approach for brain image registration with local constraints," *Integr. Comput.-Aided Eng.*, vol. 24, no. 1, pp. 73–85, 2017.

[11] K.-B. Lee, M.-S. Ko, J.-J. Lee, T.-M. Koo, and K.-H. Park, "Defect detection method for TFT-LCD panel based on saliency map model," in *Proc. TENCON*, Nov. 2004, pp. 223–226.

[12] R. R. Naraghi, L. G. Cançado, F. Salazar-Bloise, and A. Dogariu, "Near-field coherence reveals defect densities in atomic monolayers," *Optica*, vol. 4, no. 5, pp. 527–531, 2017.

[13] W. C. Chuang and S. T. Lee, "Automatic detection of special defects of non-uniformity on carbon nanotube backlight units," *J. Technol.*, vol. 22, no. 4, pp. 335–341, 2007.

[14] H. Konishi, N. Nagasawa, Y. Takahama, and M. Yamana, "Automatic focal-point sensing apparatus sensing high and low magnification," U.S. Patent 5 245 173, Sep. 14, 1993.

[15] Y. Cheng *et al.*, "Multi-layer auto-focusing system using image processing on laser reflective pattern," in *Proc. IEEE Int. Conf. Oxide Mater. Electron. Eng. (OMEE)*, 2012.

[16] G. Yang and B. J. Nelson, "Wavelet-based autofocusing and unsupervised segmentation of microscopic images," in *Proc. IEEE/RSJ Int. Conf. Intell. Robots Syst.*, vol. 3, Oct. 2003, pp. 2143–2148.

[17] A. Erteza, "Sharpness index and its application to focus control," *Appl. Opt.*, vol. 15, no. 4, pp. 877–881, 1976.

[18] J. M. Reed and S. Hutchinson, "Image fusion and subpixel parameter estimation for automated optical inspection of electronic components," *IEEE Trans. Ind. Electron.*, vol. 43, no. 3, pp. 346–354, Jun. 1996.

[19] W. Kesseler and J. Fischer, "Analytical model of autofocus systems with CCD camera," *Proc. SPIE, Sensors Camera Syst. Sci., Ind., Digit. Photogr. Appl.*, vol. 3965, pp. 369–380, May 2000.

[20] B. C. Jiang, C.-C. Wang, and H.-C. Liu, "Liquid crystal display surface uniformity defect inspection using analysis of variance and exponentially weighted moving average techniques," *Int. J. Prod. Res.*, vol. 43, no. 1, pp. 67–80, 2005.

[21] D. Mayerich, L. Abbott, and B. McCormick, "Knife-edge scanning microscopy for imaging and reconstruction of three-dimensional anatomical structures of the mouse brain," *J. Microscopy*, vol. 231, no. 1, pp. 134–143, 2008.
[22] T. C. Strand, "Optical three-dimensional sensing for machine vision," *Opt. Eng.*, vol. 24, no. 1, 1985, Art. no. 240133.
[23] A. Lasinski, A. Obotnine, and A. Weiss, "Method and apparatus for the auto-focussing infinity corrected microscopes," U.S. Patent 7 700 903, 2010.
[24] S. H. Wang, C. J. Tay, C. Quan, H. M. Shang, and Z. F. Zhou, "Laser integrated measurement of surface roughness and micro-displacement," *Meas. Sci. Technol.*, vol. 11, no. 5, pp. 454–458, 2000.
[25] C.-S. Liu, P.-H. Hu, and Y.-C. Lin, "Design and experimental validation of novel optics-based autofocusing microscope," *Appl. Phys. B, Lasers Opt.*, vol. 109, no. 2, pp. 259–268, 2012.
[26] G. C. Birch, J. S. Tyo, and J. Schwiegerling, "Depth measurements through controlled aberrations of projected patterns," *Opt. Express*, vol. 20, no. 6, pp. 6561–6574, 2012.
[27] N. Chernov and C. Lesort, "Least squares fitting of circles," *J. Math. Imag. Vis.*, vol. 23, no. 3, pp. 239–252, Nov. 2005.
[28] Z. Liu and D. Krys, "The use of laser range finder on a robotic platform for pipe inspection," *Mech. Syst. Signal Process.*, vol. 31, pp. 246–257, Aug. 2012.
[29] X. Xiong, A. Adan, B. Akinci, and D. Huber, "Automatic creation of semantically rich 3d building models from laser scanner data," *Autom. Construct.*, vol. 31, pp. 325–337, May 2013.
[30] P. Perona and J. Malik, "Scale-space and edge detection using anisotropic diffusion," *IEEE Trans. Pattern Anal. Mach. Intell.*, vol. 12, no. 7, pp. 629–639, Jul. 1990.
[31] S.-M. Chao and D.-M. Tsai, "An improved anisotropic diffusion model for detail- and edge-preserving smoothing," *Pattern Recognit. Lett.*, vol. 31, no. 13, pp. 2012–2023, 2010.
[32] N. Otsu, "A threshold selection method from gray-level histograms," *Automatica*, vol. 11, nos. 285–296, pp. 23–27, 1975.
[33] I. Hirokazu, Y. Nobuyuki, M. Ichizo, N. Fuji, M. Kazuhiko, and O. Masato, "C language digital image processing," CHUAN HWA Book Co., LTD, 2006.
[34] I. Daubechies, *Ten Lectures on Wavelets*. Philadelphia, PA, USA: SIAM, 1992.
[35] L. R. Dice, "Measures of the amount of ecologic association between species," *Ecology*, vol. 26, no. 3, pp. 297–302, 1945.
[36] X. Huang *et al.*, "Contour tracking in echocardiographic sequences via sparse representation and dictionary learning," *Med. Image Anal.*, vol. 18, no. 2, pp. 253–271, 2014.
[37] D. P. Huttenlocher, G. A. Klanderman, and W. J. Rucklidge, "Comparing images using the Hausdorff distance," *IEEE Trans. Pattern Anal. Mach. Intell.*, vol. 15, no. 9, pp. 850–863, Sep. 1993.

Wei-Yen Hsu received the Ph.D. degree from the Department of Computer Science and Information Engineering, National Cheng Kung University, Tainan, Taiwan, in 2008.

He is currently a Professor with the Department of Information Management, National Chung Cheng University. His research interests include image processing, pattern recognition, and machine learning.

Dr. Hsu is currently a Founding Member of the Brain–Computer Interface Society. He was a recipient of the Young Scholar Award from Taipei Medical University in 2011, and the Young Scholar Award and the Outstanding Research Award from National Chung Cheng University in 2013 and 2019, respectively. He is an Associate Editor of two journals, *Medicine* and *BMC Medical Informatics and Decision Making*.